International Journal of Heat and Mass Transfer 92 (2016) 467–482

Contents lists available at ScienceDirect

International Journal of Heat and Mass Transfer

journal homepage: www.elsevier.com/locate/ijhmt

Consolidated methodology to predicting flow boiling critical heat flux for inclined channels in Earth gravity and for microgravity

Chirag R. Kharangate, Christopher Konishi, Issam Mudawar *

Boiling and Two-Phase Flow Laboratory (PU-BTPFL), School of Mechanical Engineering, Purdue University, 585 Purdue Mall, West Lafayette, IN 47907, USA

ARTICLE INFO

Article history:
Received 9 June 2015
Accepted 5 August 2015
Available online 18 September 2015

Keywords:
Flow boiling
Critical heat flux
Inclined channels
Microgravity

ABSTRACT

The transition from single-phase to two-phase thermal systems in future space vehicles demands a thorough understanding of flow boiling critical heat flux (CHF) in reduced gravity, including microgravity. This study is a comprehensive, consolidated investigation of the complex trends of flow boiling CHF in a rectangular channel in both microgravity and for different orientations in Earth gravity. It is shown that the *Interfacial Lift-off Model* provides good predictions of CHF data for both gravitational environments and both single-sided and double-sided heating. CHF mechanism in Earth gravity is shown to be highly sensitive to flow orientation at very low velocities, but is consistent with the wavy vapor layer depiction of the *Interfacial Lift-off Model* at high velocities. The model predicts a stable vapor-liquid interface for downflow with a downward-facing heated wall at lower velocities, and wavy interface with a critical wavelength that decreases with increasing velocity at higher velocities. Predicted CHF values for microgravity fall about midway between the maxima and minima for Earth gravity. Overall, predicted values of CHF and key interfacial parameters for all orientations in Earth gravity and for microgravity converge above ~1.5 m/s, which points to a velocity threshold above which inertia begins to effectively negate gravity effects.

1. Introduction

1.1. Two-phase thermal management

Single-phase thermal management systems have been widely used in many industrial applications. But increasing heat densities in many modern technologies are making single-phase thermal management increasingly difficult to implement, and have shifted interest to two-phase thermal management [1]. Technologies demanding intense heat removal include high performance computers, hybrid vehicle power electronics, avionics, and laser and microwave directed energy weapon systems. All these applications share a common trend of increasing rate of heat removal from small surface areas. The effectiveness of two-phase thermal management schemes for these applications stems from their ability to capitalize upon latent heat of the coolant rather than sensible heat alone, providing orders of magnitude enhancement in heat transfer coefficient compared to single-phase schemes.

Another important attribute of two-phase thermal management is flexibility in selecting a flow configuration that is compatible with the geometrical and packaging needs of the heat dissipating device or system. This includes pool boiling thermosyphons, channel flow boiling, jet-impingement and spray [1], with emphasis placed on very high flux cooling schemes [2–4]. Channel flow boiling consists of mounting heat dissipating devices in a linear fashion along the walls of a flow channel. This configuration is both very versatile and compatible with packaging practices in many applications. More recently, researchers determined that the cooling performance in channel flow boiling can be greatly ameliorated by reducing the hydraulic diameter of the flow channel, i.e., by using mini/micro-channel flow boiling [1,5,6].

1.2. Critical heat flux (CHF) limit

The afore-mentioned ability of two-phase cooling schemes is realized within the nucleate boiling regime, which capitalizes on high frequency formation, growth, and departure of vapor bubbles from the heat-dissipating wall, while also requiring continued replenishment of the surface with bulk liquid to compensate for the liquid that is consumed at the wall by evaporation. Critical heat flux (CHF) is arguably the most important limit for two-phase cooling schemes, and is closely associated with cessation of bulk liquid access to the surface. With the nucleate boiling process

* Corresponding author. Tel.: +1 (765) 494 5705; fax: +1 (765) 494 0539.
E-mail address: mudawar@ecn.purdue.edu (I. Mudawar).
URL: https://engineering.purdue.edu/BTPFL (I. Mudawar).

http://dx.doi.org/10.1016/j.ijheatmasstransfer.2015.08.018
0017-9310/

Nomenclature

A	channel flow area
A_k	flow area for phase k
b	ratio of wetting front length to wavelength
$C_{f,i}$	interfacial friction factor
CHF	critical heat flux, q''_m
c_p	specific heat at constant pressure
c_r	real component of wave speed
D	hydraulic diameter of flow channel
D_k	hydraulic diameter for phase k
G	mass velocity
g	gravity
g_e	Earth's gravity
g_n	component of gravity normal to heater wall
H	height of flow channel's cross-section
H_a	heated wall a
H_b	heated wall b
h_{fg}	latent heat of vaporization
k_c	critical wave number
L_d	development length of flow channel
L_e	exit length of flow channel
L_h	heated length of flow channel
$\dot{m}$	mass flow rate
MAE	mean absolute error
p	pressure
P_i	interfacial perimeter
p_{in}	pressure at inlet to heated portion of channel
P_w	wall friction perimeter
q''_m	critical heat flux (CHF)
q''_w	wall heat flux
Re	Reynolds number
T	temperature
T_{in}	temperature at inlet to heated portion of channel
T_{out}	temperature at outlet from heated portion of channel
T_{sat}	saturation temperature
$\Delta T_{sub,in}$	inlet subcooling, $T_{sat} - T_{in}$
$\Delta T_{sub,out}$	outlet subcooling, $T_{sat} - T_{out}$
U	mean inlet liquid velocity
W	width of flow channel and heated walls
x	quality
x_e	thermodynamic equilibrium quality
y	coordinate perpendicular to heated wall
z	axial coordinate
z_0	axial coordinate where $U_g = U_f$
z^*	axial location for determining vapor layer thickness and critical wavelength in *Interfacial Lift-off Model*

Greek Symbols

α	vapor void fraction
δ	mean thickness of vapor layer
δ_a	mean thickness of vapor layer generated along heated wall H_a
δ_b	mean thickness of vapor layer generated along heated wall H_b
ε	heat utility ratio
η	interfacial perturbation
θ	flow orientation angle
λ_c	critical wavelength
ρ	density
ρ''	modified density
σ	surface tension
τ_i	interfacial shear stress
τ_w	wall shear stress

Subscripts

a	vapor layer generated along heated wall H_a
b	vapor layer generated along heated wall H_b
c	critical
e	Earth
exp	experimental
f	saturated liquid; bulk liquid; frictional
g	saturated vapor
ga	saturated vapor generated along heated wall H_a
gb	saturated vapor generated along heated wall H_b
i	interfacial
in	inlet to heated portion of channel
k	phase k, $k = f$ or ga or gb
out	outlet from heated portion of channel
$pred$	predicted
sat	saturation
sub	subcooling
w	heated wall (H_a or H_b)

interrupted, CHF for heat-flux-controlled surfaces is a catastrophic event, resulting in most of the heat trapped within the wall rather than rejected to the coolant, which is manifest by a rapid, unsteady rise in the wall temperature. Without a means to cut-off the power dissipation, CHF can lead to physical damage of the device being cooled by overheating or burnout. These serious consequences point to the need to both measure and accurately predict CHF.

1.3. Predictive flow boiling CHF models

Like most two-phase phenomena, researchers rely heavily on empirical correlations to predict flow boiling CHF. However, correlations are valid for specific fluids and limited ranges of operating and flow parameters, and there is great uncertainty when attempting to determine CHF for other fluids or beyond the validity range of individual parameters [7–10].

Very few theoretically based, mechanistic models have been constructed for flow boiling CHF, and these models are intended mostly for vertical upflow. As discussed in a recent review article by Konishi et al. [11] and depicted schematically in Fig. 1(a), these models are based on four competing mechanisms: *Boundary Layer Separation*, *Bubble Crowding*, *Sublayer Dryout* and *Interfacial Lift-off*. Postulated by Kutateladze and Leont'ev [12], the *Boundary Layer Separation Model* is based on analogy between vapor production and gas injection from a permeable wall into a turbulent boundary layer. In the same manner a turbulent boundary layer is separated when the injection velocity exceeds a threshold value, CHF is postulated to occur when the rate of vapor production perpendicular to the wall is increased to a level that greatly decreases the bulk liquid velocity near the wall, causing liquid stagnation at the wall and preventing adequate liquid replenishment of the wall. Proposed by Weisman and Pei [13], the *Bubble Crowding Model* is described by formation of a dense bubbly layer close to the wall at CHF, which renders turbulent fluctuations in the bulk liquid flow, which they postulated as the main source of liquid replenishment, too weak to penetrate the bubbly layer and reach the wall. Lee and Mudawar [14] proposed the *Sublayer Dryout Model*, which states that CHF will occur when the enthalpy of bulk liquid supplied to liquid sublayers that are trapped beneath large vapor blankets at the wall falls short of dissipating the heat supplied at the

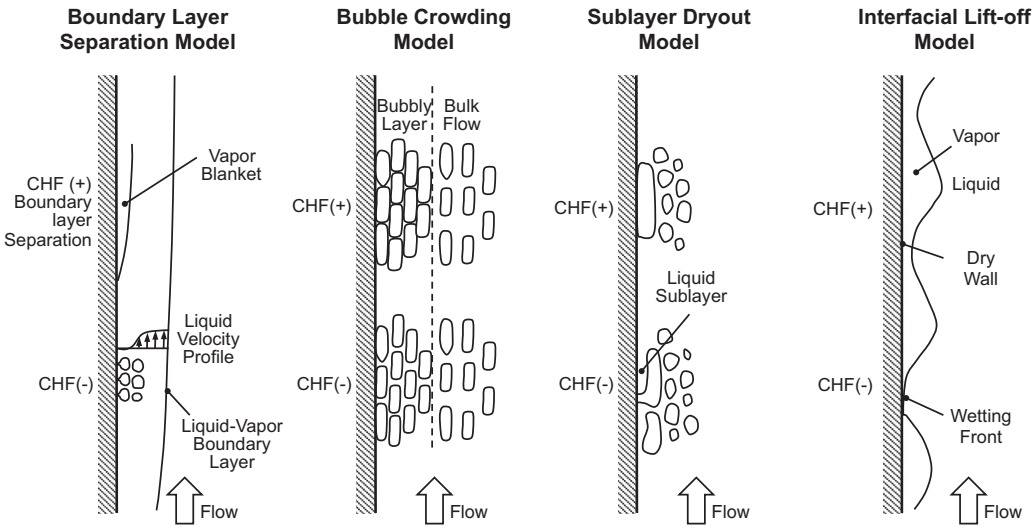

Fig. 1. (a) Trigger mechanisms for flow boiling CHF according to different models. (b) CHF transient in microgravity for FC-72 at $U = 0.15$ m/s ($\Delta T_{sub,out} = 3.0$ °C) and $U = 1.50$ m/s ($\Delta T_{sub,out} = 3.8$ °C). Adapted from [11].

wall. Galloway and Mudawar [15,16] proposed the *Interfacial Lift-off Model* based on detailed high-speed video records of interfacial features of flow boiling in a flow channel associated with CHF occurrence. Prior to CHF, vapor bubbles were observed to coalesce into a wavy vapor layer that propagated along the heated wall while allowing liquid contact with the wall in wetting fronts corresponding to the wave troughs. At CHF, intense vapor momentum in these wetting fronts caused the interface in the troughs to be lifted from the wall, extinguishing any further liquid access.

1.4. Application of flow boiling in future space systems

Future manned space missions are expected to increase in scope, size and duration. Associated with these increases will be a commensurate increase in vehicle power as well as rate of rejection of waste heat. These trends are also expected to have a profound adverse impact on the vehicle's size and weight. To tackle these issues, Fission Power Systems (FPSs), which feature both very high power and very low mass to power ratios, have been

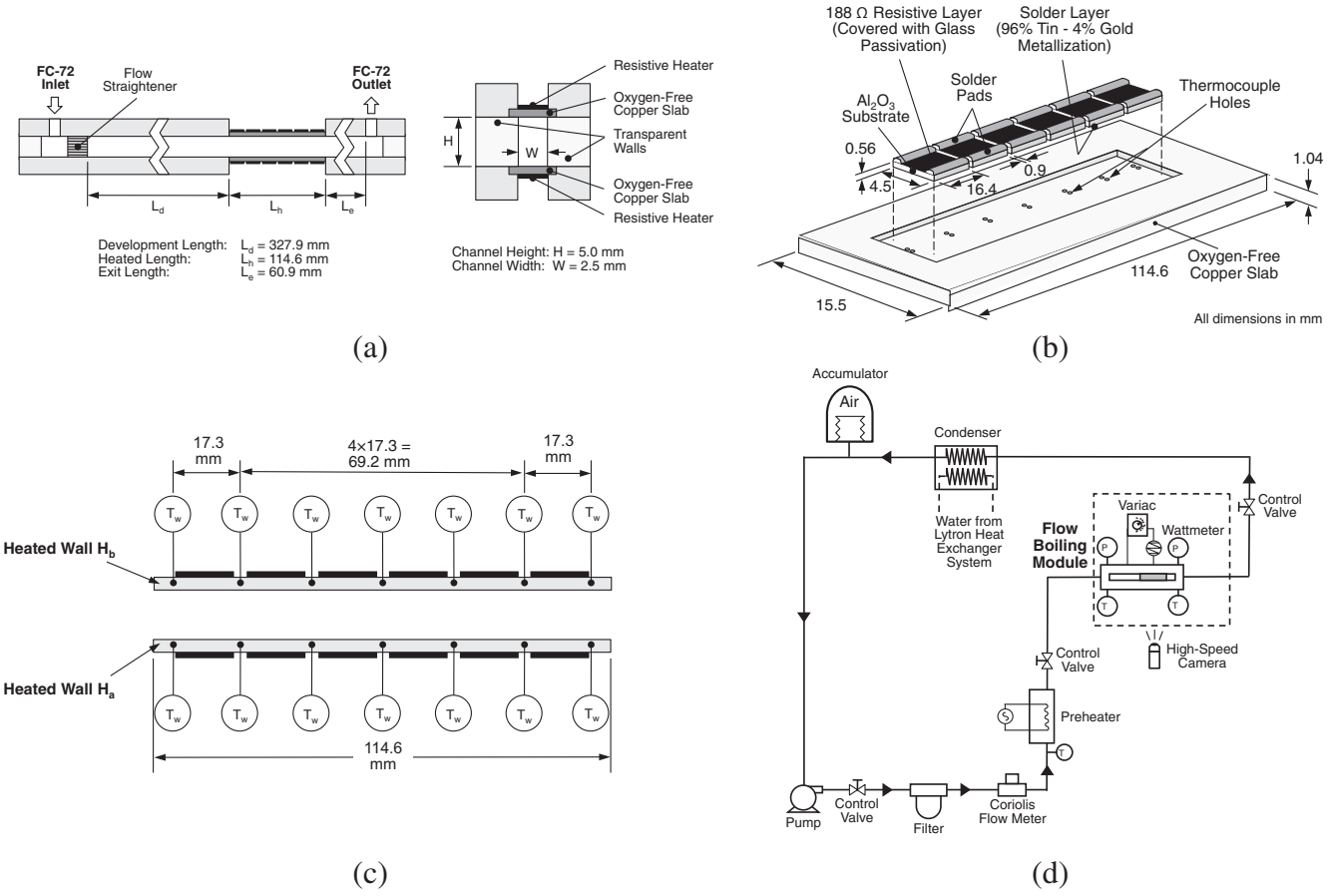

Fig. 2. (a) Key dimensions of the flow channel. (b) Construction of the heated walls and thick-film resistors. (c) Thermocouple layout in the two heated walls. (d) Schematic diagram of the flow loop.

recommended for long-duration manned missions using a Rankine power cycle [17,18]. This technology involves many complex flow boiling and condensation processes. Additional reductions in vehicle size and weight are possible by replacing present single-phase Thermal Control Systems (TCSs) with two-phase counterparts [17]. These systems play a vital role in life support in a space vehicle by controlling the temperature and humidity of the internal environment. They are comprised of three subsystems that tackle (1) *heat acquisition* from heat-dissipating sources, (2) *heat transport* from the sources, and (3) *heat rejection* to the outside environment. In most space vehicles, including space shuttles, these tasks have been tackled by a single-phase (liquid only) TCS. The two-phase TCS designs now being projected for use on future vehicles greatly decrease size and weight by capitalizing upon the orders-of-magnitude enhancement in flow boiling and condensation heat transfer coefficients compared to those possible with a single-phase TCS.

The transition to two-phase technologies requires a thorough understanding of two-phase flow and both flow boiling and condensation heat transfer in reduced gravity, especially microgravity. Reduced gravity can be simulated in a number of platforms, including above ground Drop Towers or below ground Drop Shafts, Sounding Rockets and Parabolic Flight Aircraft [17,18]. The latter has been especially popular for their ability to provide 15–30 s of microgravity, perform multiple tests in a single flight, and ability to accommodate larger experiment packages and permit direct interaction of the operator with the experimental package; they can also simulate both Lunar and Martian gravities. The International Space Station (ISS) provides an ideal environment for microgravity two-phase flow and heat transfer experiments, providing long test durations, operator access, and both automatic and remote control capabilities. Unfortunately ISS experiments are both very expensive and require many years of development and safety certification.

The vast majority of published works concerning two-phase flow and heat transfer comes from parabolic flight experiments. These include a number of adiabatic two-phase flow studies, such as those of Dukler et al. [19], Colin et al. [20], Reinarts [21], Bousman et al. [22,23], and Choi et al. [24] that were aimed at understanding the influence of microgravity on two-phase flow patterns as well as the transitions between different flow patterns. Parabolic flight flow boiling studies include flow patterns in both subcooled and saturated flow boiling by Misawa [25], impact of bubble detachment and coalescence on flow pattern development by Saito et al. [26] and Ohta et al. [27], flow boiling frictional pressure drop in flow boiling by Brutin et al. [28], and subcooled flow boiling heat transfer and CHF by Ma and Chung [29]. More recently, a collaborative effort between the Purdue University Boiling and Two-Phase Flow Laboratory (PU-BTPFL) and NASA Glenn Research Center has been focussed mostly on flow boiling CHF. Findings from this specific effort will be discussed later in this paper.

Aside from the high-cost microgravity platforms, researchers often capitalize upon the relative simplicity and low cost of testing in Earth gravity. The effects of reduced gravity on flow boiling are simulated by tilting the flow channel relative to Earth gravity. This yields a reduced component of gravity perpendicular to the heated wall. But a primary limitation with these tests is the inability to

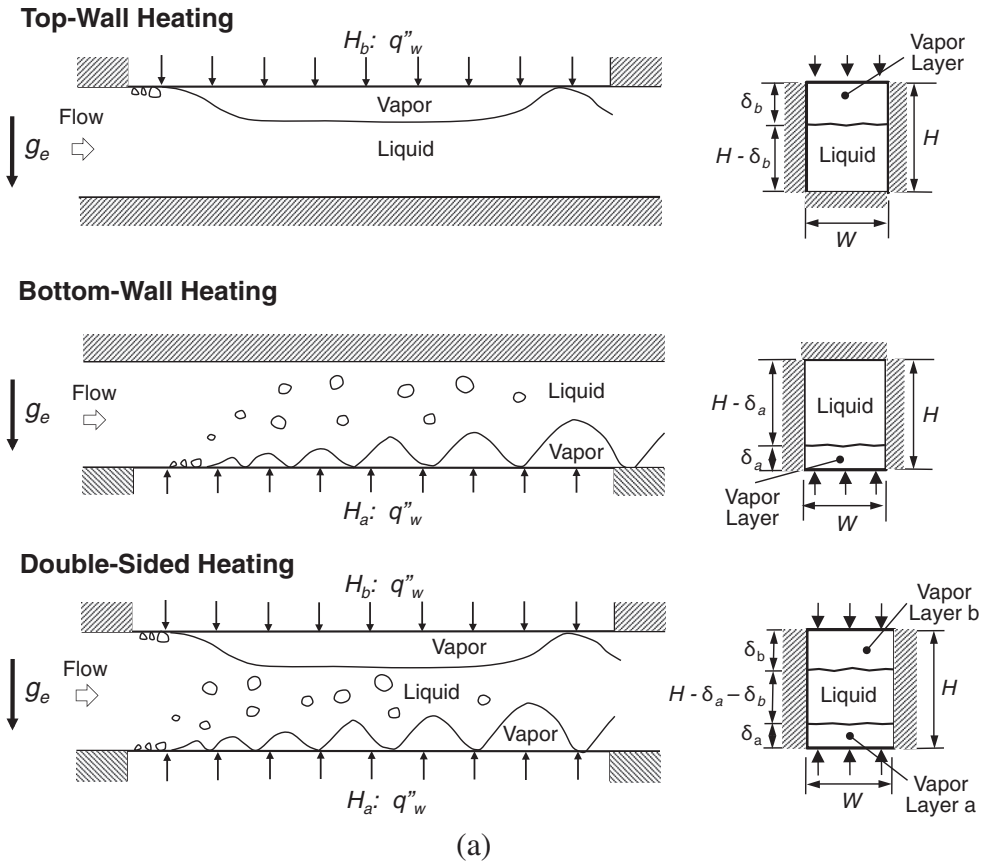

(a)

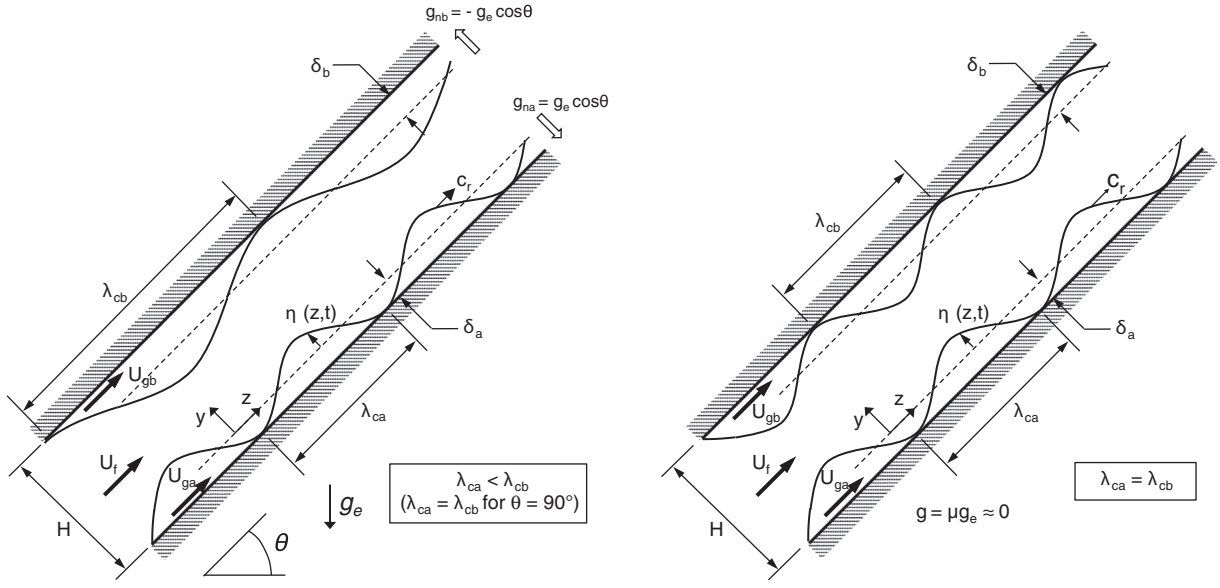

(b)

Fig. 3. (a) Depiction of horizontal flow boiling near CHF for a rectangular channel with top-wall heating, bottom-wall heating, and double-sided heating (adapted from [35]). (b) Hydrodynamic instability of wavy vapor layers along heated walls of double-sided heated channel at CHF– for inclined channel in Earth gravity and for microgravity (adapted from [40]).

isolate the influence of this gravity component and simultaneously eliminate the component of gravity along the direction of fluid flow. Nonetheless, this testing approach is widely used to amass large data bases and video records in pursuit of a mechanistic model for the influence of gravity on both pool boiling [30] and flow boiling CHF; the latter will be discussed in detail in the present paper. Investigators at PU-BTPFL have adopted this testing approach to complement parabolic flight tests in an attempt to acquire a comprehensive understanding of the influence of gravity on flow boiling CHF.

Table 1
Summary of separated flow model and *Interfacial Lift-off Model* relations for single-sided heating (Zhang et al. [33]).

Momentum conservation:

$$G^2\frac{d}{dz}\left[\frac{(1-x_a)^2}{\rho_f(1-\alpha_a)}\right] = -(1-\alpha_a)\frac{dp}{dz} - \frac{\tau_{w,f}P_{w,f}}{A} \pm \frac{\tau_{ia}P_{ia}}{A} - \rho_f(1-\alpha_a)g\sin\theta$$

$$G^2\frac{d}{dz}\left[\frac{x_a^2}{\rho_g\alpha_a}\right] = -\alpha_a\frac{dp}{dz} - \frac{\tau_{w,ga}P_{w,ga}}{A} \mp \frac{\tau_{ia}P_{ia}}{A} - \rho_g\alpha_g g\sin\theta$$

Energy conservation:

$$\frac{dx_a}{dz} = \frac{q''_w W}{\dot{m}(c_{p,f}\Delta T_{sub,in} + h_{fg})}$$

Critical wavelength:

$$k_{ca} = \frac{2\pi}{\lambda_{ca}} = \frac{\rho''_{fa}\rho''_{ga}(U_{ga}-U_f)^2}{2\sigma(\rho''_{fa}+\rho''_{ga})} + \sqrt{\left[\frac{\rho''_{fa}\rho''_{ga}(U_{ga}-U_f)^2}{2\sigma(\rho''_{fa}+\rho''_{ga})}\right]^2 + \frac{(\rho_f-\rho_g)g_{na}}{\sigma}}$$

where the modified densities are given by

$$\rho''_{ga} = \rho_g\coth\left(\frac{2\pi}{\lambda_{ca}}\delta_a\right) \quad \text{and} \quad \rho''_{fa} = \rho_f\coth\left(\frac{2\pi}{\lambda_{ca}}(H-\delta_a)\right)$$

Critical heat flux (CHF):

$$CHF = \frac{\rho_g}{\varepsilon}(c_{p,f}\Delta T_{sub,in} + h_{fg})\left[\frac{4\pi\sigma b\sin(b\pi)}{\rho_g}\right]^{1/2}\left.\frac{\delta_a^{1/2}}{\lambda_{ca}}\right|_{z_a^*}$$

where $z_a^* = z_{0a} + \lambda_{ca}(z_a^*)$

Table 2
Summary of relations used in conjunction with the separated flow model and *Interfacial Lift-off Model* for single-sided wall heating (Zhang et al. [33]) and double-sided wall heating (Konishi et al. [40]).

Single-sided heating quality relation for vapor layer:

$$x_a = \frac{\rho_g U_{ga}\alpha_a}{G}$$

Double-sided heating quality relations for individual vapor layers:

$$x_a = \frac{\rho_g U_{ga}\alpha_a}{G} \quad \text{and} \quad x_b = \frac{\rho_g U_{gb}\alpha_b}{G}$$

Wall shear stress relations:

$$\tau_{w,k} = \frac{1}{2}\rho_k U_k^2 f_k$$

$$f_k = C_1 + \frac{C_2}{Re_{D_k}^{1/C_3}} = C_1 + \frac{C_2}{\left(\frac{\rho_k U_k D_k}{\mu_k}\right)^{1/C_3}}$$

where $k = f$, ga or gb. $C_1 = 0$, $C_2 = 16$ and $C_3 = 1$ for laminar flow ($Re_{D_k} \leqslant 2100$), $C_1 = 0.0054$, $C_2 = 2.3\times10^{-8}$ and $C_3 = -2/3$ for transitional flow ($2100 < Re_{D_k} \leqslant 4000$), and $C_1 = 0.00128$, $C_2 = 0.1143$ and $C_3 = 3.2154$ for turbulent flow ($Re_{D_k} > 4000$), where $D_k = 4A_k/P_k$

Interfacial shear stress relations:

$$\tau_{ia} = \frac{C_{f,ia}}{2}\rho_g(U_{ga}-U_f)^2 \quad \text{and} \quad \tau_{ib} = \frac{C_{f,ib}}{2}\rho_g(U_{gb}-U_f)^2$$

where $C_{f,ia} = C_{f,ib} = 0.5$
Heat utility ratio:

$$\varepsilon = 1 - 0.00285\frac{\rho_f}{\rho_g}\frac{c_{p,f}\Delta T_{sub,out}}{h_{fg}}\left(\frac{\rho_f U^2 D}{\sigma}\right)^{0.2}$$

1.5. Influence of fluid flow and heated wall orientations on CHF

Aside from enabling the study of reduced gravity influence on flow boiling, experiments performed by tilting the flow channel relative to Earth gravity also provide the flexibility of one-sided or two-sided wall heating. While these two wall heating configurations can greatly complicate the influence of gravity on CHF, they also provide the opportunity for a more detailed mechanistic assessment of this influence. This assessment is a key objective of the present study.

Single-sided heating is borne out of the need to simulate cooling of electronic or power sources using flow boiling in a rectangular channel [31,32]. Using similar single-sided heating, Zhang et al. [33] studied the influence of flow orientation on CHF for subcooled inlet conditions. Using FC-72 as working fluid, they showed that the influence of orientation, and therefore gravity, on CHF diminishes monotonically with increasing flow velocity, becoming virtually independent of orientation above a threshold of 1.5 m/s. Similar trends were measured by Konishi et al. [34] for two-phase inlet conditions, $x_{e,in} \geqslant 0$. Kharangate et al. [35,36] studied horizontal flow of FC-72 in a rectangular channel with both bottom wall heating and top wall heating over a wide range of channel inlet conditions, ranging from highly subcooled to positive inlet quality. Both wall heating configurations had Earth gravity perpendicular to the heated wall, with gravity aiding vapor removal from the heated wall for bottom wall heating, while causing vapor accumulation along the heated wall for top wall heating. By performing similar experiments at other orientations relative Earth gravity, they were able to determine the flow velocity at which the influence of gravity on CHF becomes negligible.

Originally proposed by Galloway and Mudawar [15,16], the *Interfacial Lift-off Model* has been validated in several studies that were performed in both Earth gravity [33,34,37] and microgravity [38–40] over a wide range of operating conditions using both CHF data and high-speed video. Shown in Fig. 1(b) are images of the wavy vapor layer captured by Zhang et al. [38] before, during, and shortly after CHF for single-sided heating of FC-72 in microgravity at inlet liquid velocities of $U = 0.15$ and 1.5 m/s. These images depict the wavy vapor layer development prior to wetting front dryout that accompanies CHF occurrence.

1.6. Objective of study

As indicated above, flow boiling CHF in a rectangular channel is sensitive to flow velocity, orientation and whether the channel is heated along one side or both sides. The primary goal of the present study is to model, for all flow orientations, the complex influence of Earth gravity components perpendicular to the heated wall and parallel to the direction of fluid flow on CHF for FC-72 in a rectangular channel with single-sided and double-sided heating. It will be shown how the *Interfacial Lift-off Model* possesses both the flexibility and rigor to predict the effects of flow velocity and wall

Table 3
Summary of separated flow model and *Interfacial Lift-off Model* relations for double-sided heating (Konishi et al. [40]).

Momentum conservation:

$$G^2\frac{d}{dz}\left[\frac{(1-x_a-x_b)^2}{\rho_f(1-\alpha_a-\alpha_b)}\right]=-(1-\alpha_a-\alpha_b)\frac{dp}{dz}-\frac{\tau_{w,f}P_{w,f}}{A}\pm\frac{\tau_{ia}P_{ia}}{A}\pm\frac{\tau_{ib}P_{ib}}{A}-\rho_f(1-\alpha_a-\alpha_b)g\sin\theta$$

$$G^2\frac{d}{dz}\left[\frac{x_a^2}{\rho_g\alpha_a}\right]=-\alpha_a\frac{dp}{dz}-\frac{\tau_{w,ga}P_{w,ga}}{A}\mp\frac{\tau_{ia}P_{ia}}{A}-\rho_g\alpha_a g\sin\theta$$

$$G^2\frac{d}{dz}\left[\frac{x_b^2}{\rho_g\alpha_b}\right]=-\alpha_b\frac{dp}{dz}-\frac{\tau_{w,gb}P_{w,gb}}{A}\mp\frac{\tau_{ib}P_{ib}}{A}-\rho_g\alpha_b g\sin\theta$$

Energy conservation:

$$\frac{dx_a}{dz}=\frac{dx_b}{dz}=\frac{q''_wW}{\dot{m}(c_{p,f}\Delta T_{sub,in}+h_{fg})}$$

Critical wavelength:

$$k_{cm}=\frac{2\pi}{\lambda_{cm}}=\frac{\rho''_{fm}\rho''_{gm}(U_{gm}-U_f)^2}{2\sigma(\rho''_{fm}+\rho''_{gm})}+\sqrt{\left[\frac{\rho''_{fm}\rho''_{gm}(U_{gm}-U_f)^2}{2\sigma(\rho''_{fm}+\rho''_{gm})}\right]^2+\frac{(\rho_f-\rho_g)g_{nm}}{\sigma}}$$

where the modified densities are given by

$$\rho''_{gm}=\rho_g\coth\left(\frac{2\pi}{\lambda_{cm}}\delta_m\right)\quad\text{and}\quad\rho''_{fm}=\rho_f\coth\left(\frac{2\pi}{\lambda_{cm}}(H-\delta_a-\delta_b)\right)$$

$m = a$ for heater H_a and $m = b$ for heater H_b

Critical heat flux (CHF):

$$CHF=\frac{\rho_g}{\varepsilon}(c_{p,f}\Delta T_{sub,in}+h_{fg})\left[\frac{4\pi\sigma bsin(b\pi)}{\rho_g}\right]^{1/2}\left.\frac{\delta_m^{1/2}}{\lambda_{cm}}\right|_{z^*_m}$$

where $z^*_m=z_{0m}+\lambda_{cm}(z^*_m)$

heating in both Earth gravity and microgravity. The present study is a part of a NASA project that was initiated in 2012 with the ultimate goal of developing the Flow Boiling and Condensation Experiment (FBCE) for deployment in the International Space Station (ISS) in 2018.

2. Experimental methods

2.1. Flow boiling module

A flow boiling module is designed to both measure CHF and photographically investigate interfacial behavior associated with CHF occurrence. Depicted in Fig. 2(a), the module consists of three transparent polycarbonate plastic (Lexan) plates sandwiched between two aluminum support plates. Together, the three Lexan plates constitute the flow channel. The 2.5-mm wide and 5-mm high flow channel is milled into the middle Lexan plate. Rectangular slots are also milled through the top and bottom Lexan plates to accommodate two 114.6-mm long, 15.5-mm wide, and 1.04-mm thick oxygen-free copper slabs which serve as heating walls. O-rings are fitted into shallow grooves in the Lexan plates to prevent any fluid leaks from the flow channel. The flow boiling module also features a honeycomb flow straightener at the channel's inlet to break up any large inlet eddies. The flow channel has a hydrodynamic development length a hundred times the channel's hydraulic diameter.

Fig. 2(b) and (c) show the detailed construction and temperature instrumentation of the heated walls, respectively. Soldered to the backside of each copper slab are six 188-Ω, 4.5-mm wide and 16.4-mm long thick film resistors. A variable voltage source is used to power these resistors in parallel to provide uniform heat flux along each wall.

Liquid temperature is measured at the inlet port of the flow boiling module and downstream of the heated channel. Heated wall temperatures are measured by type-E thermocouples inserted in shallow holes that are drilled between the resistors at seven equidistant locations. Fig. 2(c) shows the axial positions of these thermocouples. A heated wall relay is set to automatically cut off power supply to the resistors once any of the wall temperatures exceeds 130 °C, which indicates CHF occurrence. Pressure measurements are made at three locations in the flow module: near the inlet port and just upstream and downstream of the copper slabs.

2.2. Flow loop

Fig. 2(d) shows a schematic of the two-phase flow loop. This loop is configured to supply deaerated FC-72 to the flow boiling module at prescribed flow rate, pressure and temperature. FC-72 is circulated with the aid of a magnetically coupled gear pump. Exiting the pump, the fluid is passed through a filter, Coriolis flow meter and preheater before entering the flow boiling module. Downstream from the flow boiling module, the two-phase mixture is passed through a water-cooled condenser to return any vapor to liquid state. An air-pressurized accumulator is connected to the loop between the condenser and the pump, serving the dual purpose of setting a low reference pressure point for the entire loop, as well as compensate for any fluid expansion or contraction in the loop.

2.3. Operating conditions and measurement uncertainty

The operating conditions for the present study are as follows: FC-72 inlet velocity of $U = 0.11$–2.02 m/s, inlet temperature of $T_{in} = 53.2$–67.0 °C (corresponding to inlet subcooling of $\Delta T_{sub,in} = 1.9$–8.4 °C), and inlet pressure of $p_{in} = 99.3$–161.8 kPa (14.4–23.5 psi). Fluid and heated wall temperatures throughout the facility are measured with type-E thermocouples having an accuracy of ±0.5 °C. STS absolute pressure transducers having an accuracy of ±0.05% are used to measure pressure at several locations along the flow boiling module and the flow loop. The Coriolis flow meter has an accuracy of ±0.1% and the wall heat is measured with an accuracy of ±0.5 W.

3. Interfacial Lift-off Model

Fig. 3(a) illustrates the interfacial complexity resulting from wall heating configuration (top-wall heating, bottom-wall heating, double-sided heating) for horizontal flow in Earth gravity. Clearly, more complex flow regimes are encountered in other orientations, and it is the goal of this section to utilize the *Interfacial Lift-off Model* to explore the influence of flow orientation, flow velocity and heating configuration on interfacial instability, as well as to predict CHF.

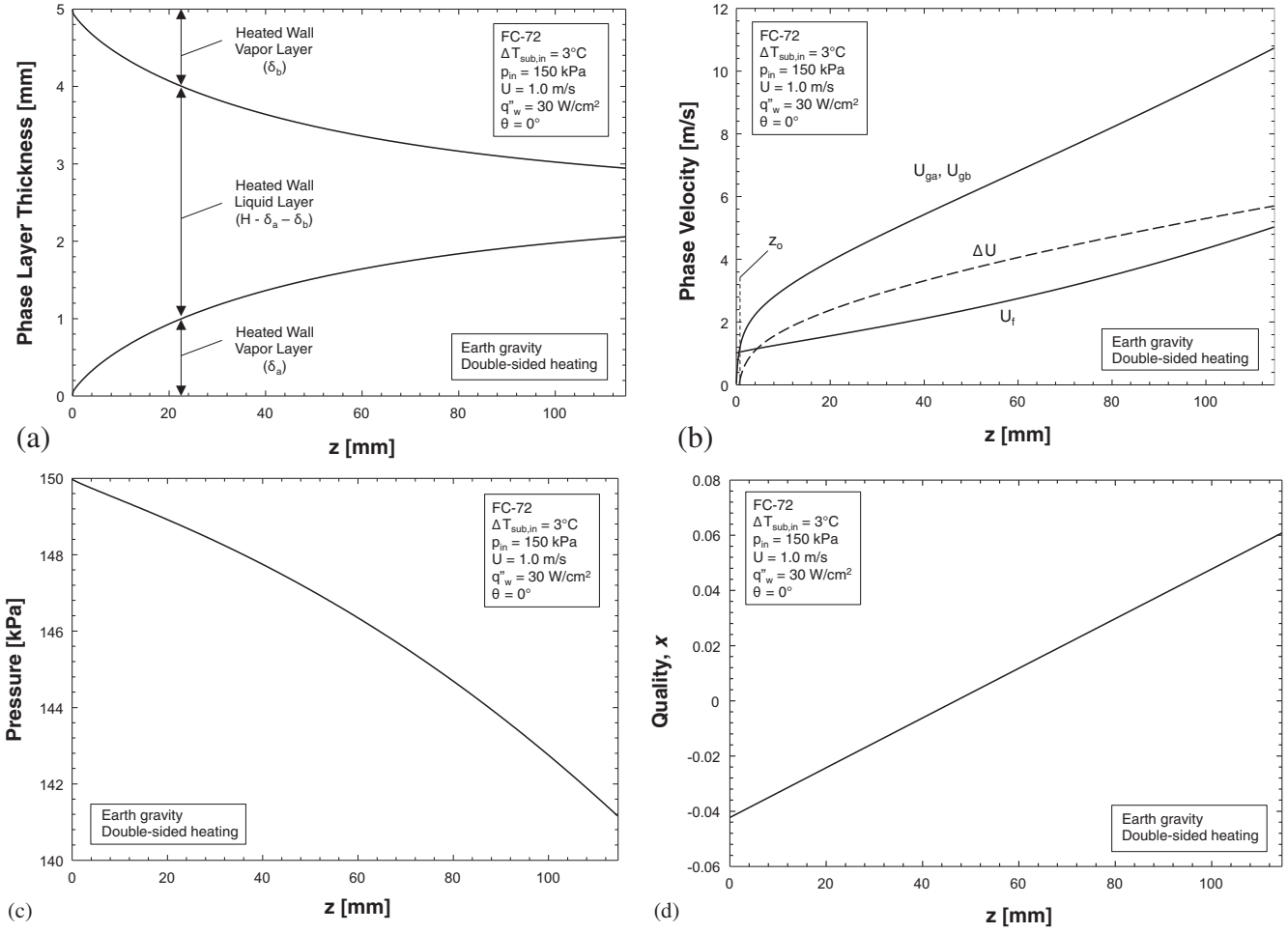

Fig. 4. Separated flow model predictions of (a) phase layer thicknesses, (b) phase velocities, (c) pressure, and (d) quality.

3.1. Single-sided heating

Zhang et al. [33] developed a control-volume-based separated flow model for single-sided heating. As subcooled liquid enters the heated section of the channel, a vapor film begins to form near the leading edge. Due to phase change occurring along the channel, the vapor layer grows monotonically in thickness in the axial direction. The model is based on slip flow assumptions, i.e., uniform velocity in the liquid and vapor layers, while allowing for velocity differences between the two layers. The separated flow model also assumes pressure is uniform across the flow area. This model is used to determine the variations of mean velocities and thicknesses of the liquid and vapor layers along the channel. These parameters are used to determine the critical wavelength for instability of the vapor layer. For an unstable interface along heated wall H_a, the critical wavelength, λ_{ca}, is given by

$$k_{ca} = \frac{2\pi}{\lambda_{ca}} = \frac{\rho''_{fa}\rho''_{ga}(U_{ga}-U_f)^2}{2\sigma(\rho''_{fa}+\rho''_{ga})} + \sqrt{\left[\frac{\rho''_{fa}\rho''_{ga}(U_{ga}-U_f)^2}{2\sigma(\rho''_{fa}+\rho''_{ga})}\right]^2 + \frac{(\rho_f-\rho_g)g_{na}}{\sigma}}, \quad (1)$$

where ρ''_{fa}, ρ''_{ga}, U_f, U_{ga} and g_{na} are the modified liquid density, modified vapor density, mean velocity of the liquid layer, mean velocity of the wavy vapor layer, and component of gravity normal to the heated wall; the latter given by

$$g_{na} = g_e \cos\theta, \quad (2)$$

Using the *Interfacial Lift-off Model*, Zhang et al. [33] determined CHF according to the relation

$$CHF = q''_m = \frac{\rho_g}{\varepsilon}(c_{p,f}\Delta T_{sub,in} + h_{fg})\left[\frac{4\pi\sigma b\sin(b\pi)}{\rho_g}\right]^{1/2}\left.\frac{\delta_a^{1/2}}{\lambda_{ca}}\right|_{z_a^*}, \quad (3)$$

where b, ε, δ_a and z_a^* are the ratio of wetting front length to critical wavelength, heat utility ratio, mean vapor layer thickness along heated wall H_a, and axial location where vapor layer thickness and critical wavelength are determined. CHF for horizontal flow with bottom-wall and top-wall heating is calculated by setting $\theta = 0°$ and 180°, respectively. The key equations for the CHF model for single-sided heating are provided in Tables 1 and 2.

3.2. Double-sided heating

Konishi et al. [40] extended the model by Zhang et al. [33] to double-sided heating for subcooled inlet conditions. As subcooled liquid enters the heated section of the channel, two vapor layers begin to form at the leading edges of both heated walls surrounding a middle liquid layer. Using slip flow assumptions similar to those adopted for single-sided heating, momentum and energy conservation relations are used to determine mean velocities and thicknesses for the three layers. Critical wavelength is calculated using the same relation as for single-sided heating, the major

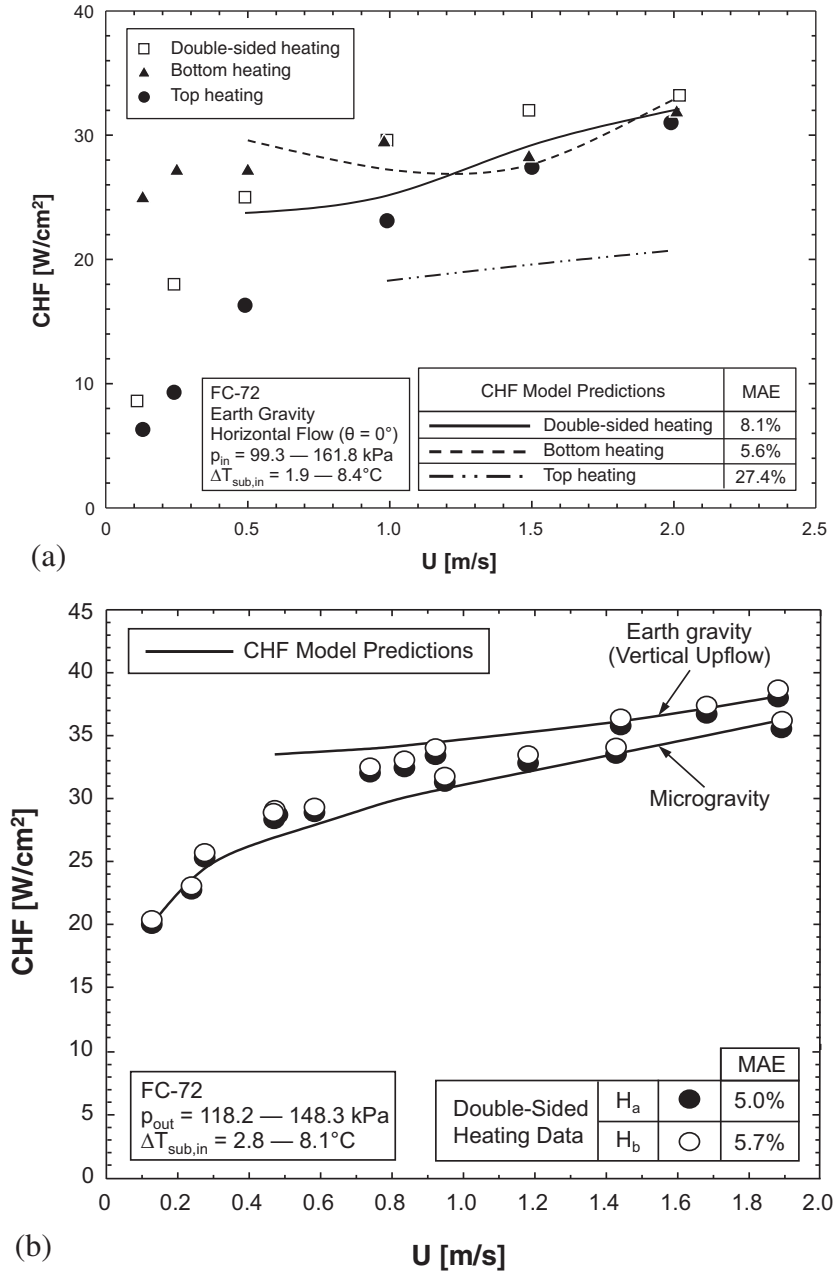

Fig. 5. Comparison of *Interfacial Lift-off Model* predictions to CHF data for (a) horizontal top-wall, bottom-wall and double-sided heating in Earth gravity, and (b) double-sided heating in microgravity and vertical upflow in Earth gravity ((b) adapted from [40]).

difference being gravity components perpendicular to the heated wall. In Earth gravity, the gravity components normal to the upward-facing heated wall and downward-facing heated wall are expressed, respectively, as

$$g_{na} = g_e \cos\theta \tag{4a}$$

and

$$g_{nb} = g_e \cos(\theta + \pi) = -g_e \cos\theta. \tag{4b}$$

The differences in critical wavelength between the upward-facing and downward-facing walls are illustrated in Fig. 3(b). In Earth gravity, the normal component tends to stabilize the interface along the downward-facing wall and destabilize the interface along the upward-facing wall. This causes CHF for the upward-facing wall to be larger than for the downward-facing wall. The differences in CHF decrease monotonically with increasing inlet velocity as inertia tends to overcome body force effects, ultimately leading to convergence of CHF values for the two heated wall orientations. For microgravity, identical interfacial behavior is encountered on both walls, which leads to equal CHF values regardless of inlet velocity. The key equations of the model for double-sided heating are summarized in Table 3. Table 2 provides relations used in conjunction with the separated flow model and the *Interfacial Lift-off Model* to predict CHF for both single-sided and double-sided heating.

4. Results and discussion

4.1. Separated flow model predictions

Fig. 4(a)–(d) show predictions of the separated flow model for horizontal double-sided heating in Earth gravity with U = 1.0 m/s,

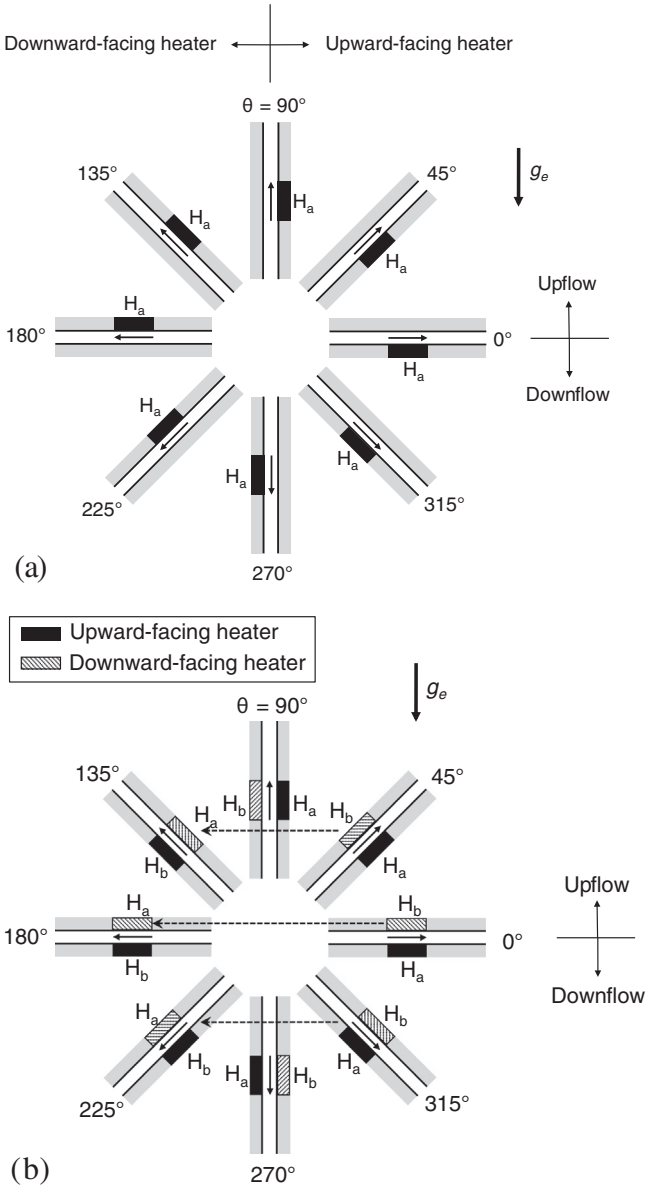

Fig. 6. Flow orientation and heater nomenclature for (a) single-sided heating and (b) double-sided heating in Earth gravity.

p_{in} = 150 kPa, $\Delta T_{sub,in}$ = 3 °C, and q''_w = 30 W/cm^2. Fig. 4(a) shows variations of thicknesses of the separated layers along the heated section of the channel. The two vapor layers are shown beginning to form at the leading edges and grow monotonically along the heated walls on the expense of a gradually consumed middle liquid layer. The phase layer thicknesses are needed to calculate the modified phase densities, ρ''_f and ρ''_g, in the relation for critical wavelength, Eq. (1). Another parameter that is important to calculating the critical wavelength is phase velocity difference. Fig. 4(b) shows the variations of the phase velocities and velocity difference between the vapor layers and middle liquid layer. The liquid layer is faster than the two vapor layers at $z = 0$, but is quickly overtaken by the vapor layers over a short distance from the leading edges of the heated walls. The distance where the vapor layers overtake the liquid layer is $z = z_o$, which is an important parameter in the *Interfacial Lift-off Model*. Fig. 4(c) and (d) show predictions of pressure and quality, respectively, along the heated section of the channel. Notice that the equilibrium quality starts with a negative value at $z = 0$ because of the subcooled inlet conditions but becomes positive downstream along the heated section.

The results from the separated flow model are used to compute CHF. Because the heated walls face opposite orientations of the perpendicular component of Earth gravity, two different CHF values are determined, one for each heated wall. Even though the model predicts two CHF values, only the lower of the two is physically relevant since, in the actual experiments, power input to both heated walls is cut off once CHF is detected in either wall.

4.2. CHF predictions

To assess the effectiveness of the *Interfacial Lift-off Model*, predictions are compared to experimental data for single-sided and double-sided heating in both Earth gravity and microgravity. Fig. 5(a) compares CHF predictions to experimental horizontal flow data for single-sided and double-sided heating in Earth gravity for slightly subcooled inlet conditions. The model predicts a stable interface below U = 1.0 and 0.5 m/s for top-wall heating and double-sided heating configurations, respectively, and an unstable interface for bottom-wall single-sided heating. A stable interface, which will be discussed later in this study, corresponds to low CHF values beyond the validity range of the *Interfacial Lift-off Model*. In two separate studies, Kharangate et al. [35,36] showed that bottom-wall heating below U = 0.5 m/s yields conditions resembling pool boiling that are dominated by gravity, and for which the wavy vapor layer is not observed. The velocity ranges associated with a stable interface ($U \leqslant$ 1.0 m/s for top-wall heating and $U \leqslant$ 0.5 m/s for double-sided heating) and pool boiling behavior ($U \leqslant$ 0.5 m/s for bottom-wall heating) impose lower limits for validity of the *Interfacial Lift-off Model*, as indicated in Fig. 5(a). Above these velocity limits, the predictive accuracy of the model is accessed using mean absolute error (MEA), which is defined as

$$MAE = \frac{1}{N}\sum\left|\frac{CHF_{pred} - CHF_{\exp}}{CHF_{\exp}}\right|. \quad (5)$$

For bottom-wall heating and double-sided heating, Fig. 5(a) shows good model predictions both in magnitude and trend, evidences by MAEs of 5.6% and 8.1%, respectively. For bottom-wall heating, the model predicts a transition from gravity-dominated to inertia-dominated flow, with the slope of CHF versus U changing from negative to positive around 1.5 m/s. For top-wall heating, the model is able to capture the trend of CHF increasing with increasing U, albeit with a higher *MAE* of 27.4%. In a previous study by Konishi et al. [40], good agreement was demonstrated between the model predictions and experimental results for double–sided heating in both microgravity and vertical upflow in Earth gravity, as shown in Fig. 5(b). In summary, Fig. 5(a) and (b) demonstrate the effectiveness of the *Interfacial lift-off Model* in modeling both single-sided and double-sided heating in both Earth gravity and microgravity.

4.3. Liquid–vapor interfacial behavior

Fig. 6(a) and (b) show the eight flow orientations that are examined for single-sided and double-sided heating in Earth gravity. For all these orientations, the flow enters from the center and radiates outwards. The orientation angle dictates whether the channel is incurring *upflow* or *downflow* relative to Earth gravity, while the placement of the heated wall decides if the wall is *upward-facing* or *downward-facing*. Due to symmetry, double-sided heating in Earth gravity requires the flow channel to span only half a full circle (θ = 0–360°) from vertical upflow to vertical downflow to cover all orientations. But for consistency between single-sided and double-sided heating configurations, results are presented below

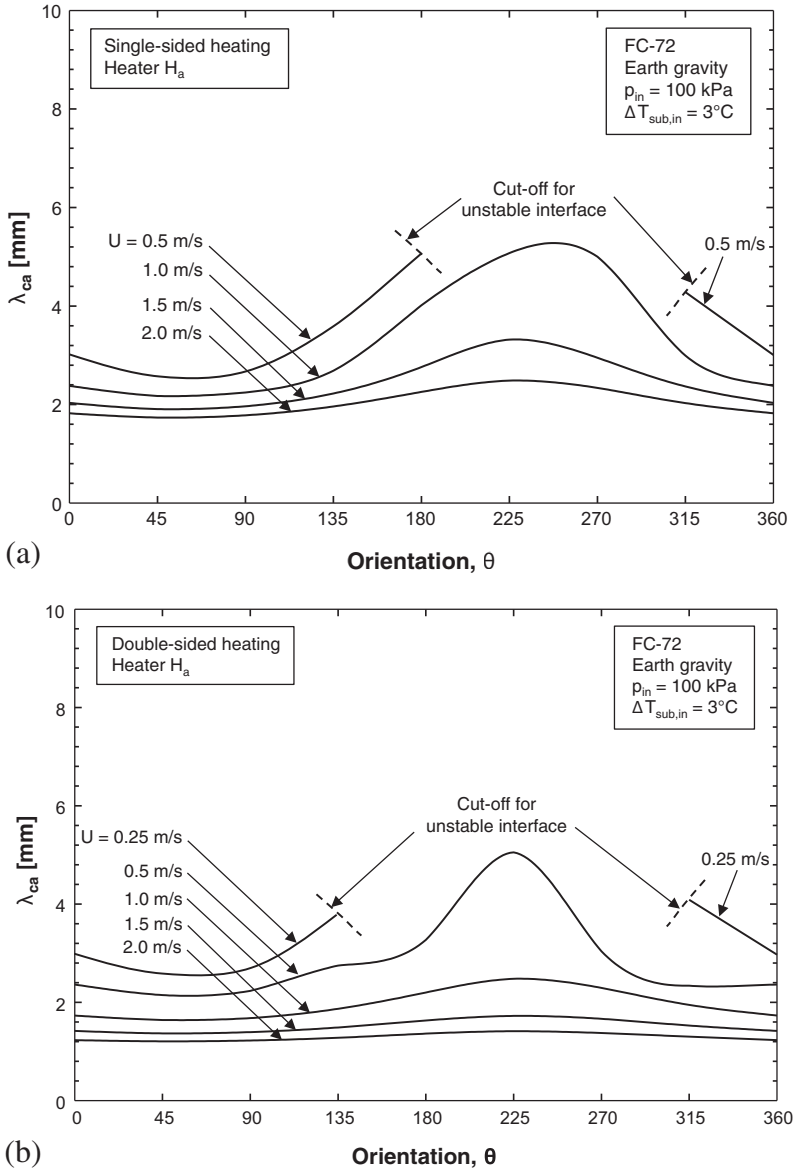

Fig. 7. Variation of predicted critical wavelength with orientation relative to Earth gravity for (a) single-sided heating and (b) double-sided heating.

for the entire range of θ = 0–360°. Fig. 6(a) and (b) indicate the locations of the heated walls H_a and H_b. For double-sided heating, Fig. 6(b) also indicates where H_a and H_b are either upward-facing or downward-facing.

As indicated earlier, Zhang et al. [33] performed extensive studies on the effects of orientation on interfacial behavior and CHF for single-sided heating in Earth gravity. They compared interfacial behavior at CHF– for $\Delta T_{sub,out}$ = 3 °C for flow velocities between U = 0.1 and 1.5 m/s. Large variations of interfacial behavior were observed with different orientation at 0.1 m/s, which should have a profound influence on CHF mechanism and magnitude. For U = 1.5 m/s, a significant increase in inertia yielded virtually identical wavy vapor layer interfacial behavior over the entire range of orientations. In a more recent study, Kharangate et al. [35] observed the same wavy vapor layer behavior for both single-sided and double-sided heating in horizontal flow in Earth gravity for $U \geqslant 1$ m/s. In another study, Konishi et al. [39] observed the same wavy vapor layer behavior for both single-sided and double-sided heating in microgravity for 0.1 < U < 1.9 m/s.

4.4. Effect of orientation on critical wavelength

The interfacial behavior captured with high-speed video and the CHF predictions provide ample support of the validity of the *Interfacial Lift-off Model*. Predicted results hereafter are obtained using the *Interfacial Lift-off Model* for FC-72 for near-saturated inlet conditions, $\Delta T_{sub,in}$ = 3 °C, and an inlet pressure of p_{in} = 100 kPa.

As discussed earlier, the critical wavelength is a key parameter of the *Interfacial Lift-off Model*. It is calculated using Eq. (1) by utilizing the liquid and vapor layer thicknesses and velocities predicted using the separated flow model. Several of the flow visualization studies discussed earlier have confirmed the existence of a wavy vapor layer along the heated wall, with contact of the bulk liquid with the wall maintained at CHF– only in wetting fronts corresponding to the wave troughs. Clearly, hydrodynamic instability of the liquid–vapor interface is crucial to formation of both the wavy vapor layer and the wetting fronts.

An iterative procedure discussed in detail by Konishi et al. [40] is adopted to calculate CHF. In this procedure, an input heat flux to

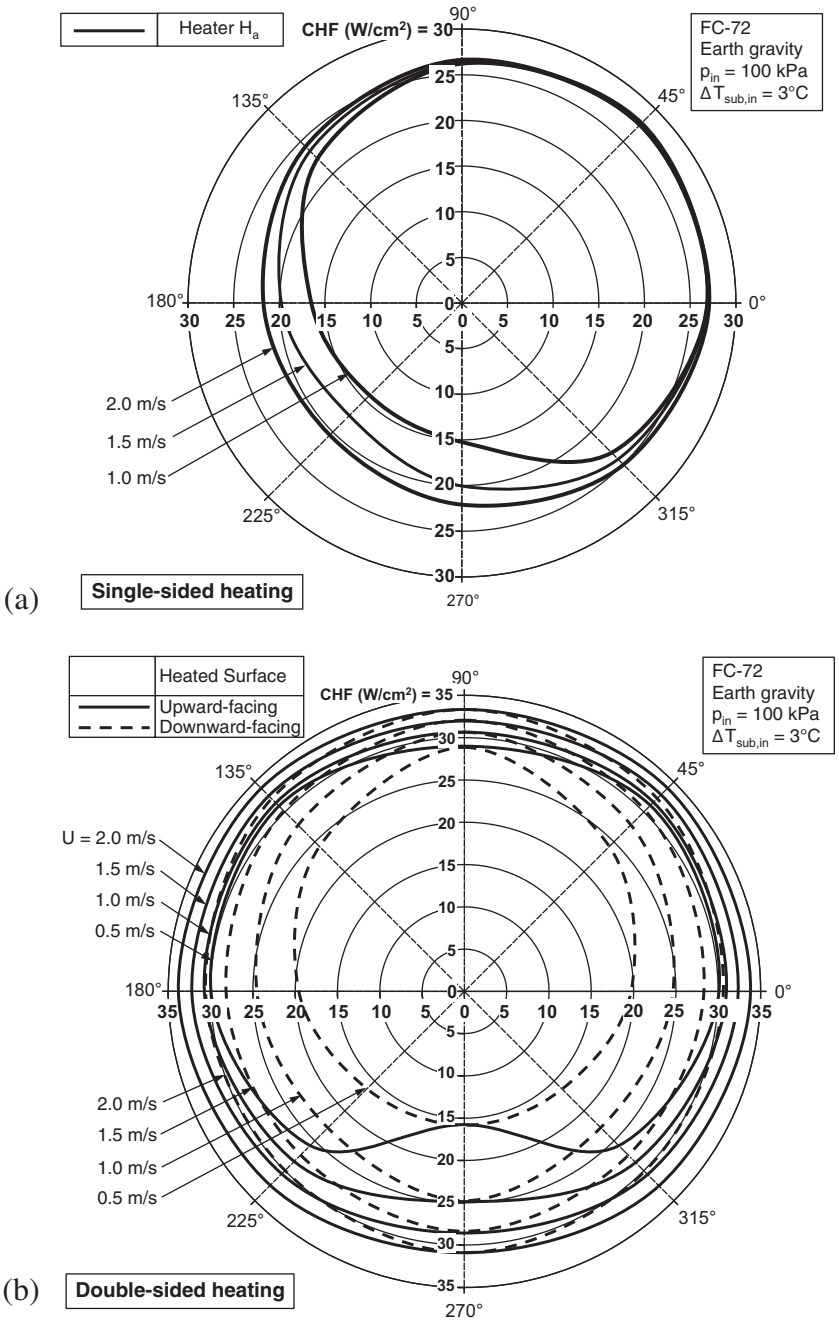

Fig. 8. Polar plots of predicted CHF with orientation relative to Earth gravity for different inlet velocities for (a) single-sided heating and (b) double-sided heating.

the heated walls is assumed, which is used to calculate the key output parameters of the separated flow model. These parameters are then used to calculate the critical wavelength and CHF using equations provided in Tables 1 and 3 for single-sided and double-sided heating, respectively. Bisection method is used to achieve convergence between the assumed heat flux and computed CHF.

In this section, this iterative procedure is used to determine the variations of critical wavelength corresponding to the convergent CHF value with orientation and velocity in Earth gravity, and with velocity in microgravity. These variations are then used to gain insight into the influence of critical wavelength on CHF trends.

Fig. 7(a) and (b) show, for different velocities, the variation of critical wavelength, λ_{ca}, for heated wall H_a with orientation relative to Earth gravity for single-sided and double-sided heating, respectively. Notice in Fig. 7(a) the existence of a region between $\theta = 180°$ and 270° for $U = 0.5$ m/s, where the interface is stable; this is where the *Interfacial Lift-off Model* is invalid. Increasing the velocity to $U = 1$ m/s, the interface becomes unstable and the critical wavelength is predicted over the entire range of orientations. Increasing the velocity further, λ_{ca} exhibits little variation with orientation. This can be explained mathematically by examining the two terms under the radical in Eq. (1), which account for inertia and gravity effects. High velocity allows inertia to dwarf gravity effects, and the second term becomes negligible, leading to convergence of λ_{ca} values for a given velocity regardless of orientation. Fig. 7(a) also shows that λ_{ca} decreases with increasing velocity, which implies wetting fronts become more remote from one another with decreasing velocity, a behavior that was confirmed experimentally by Kharangate et al. [36].

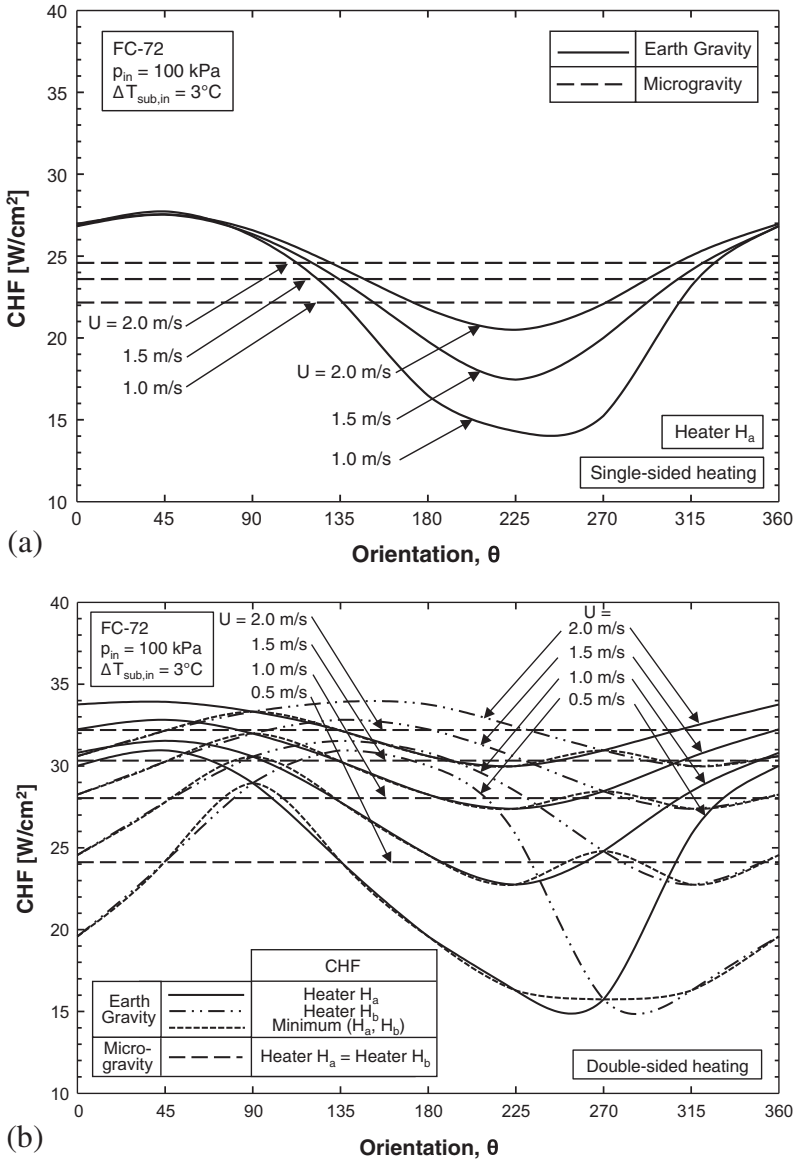

Fig. 9. Variation of predicted CHF with orientation in Earth gravity and microgravity for (a) single-sided heating and (b) double-sided heating.

Fig. 7(b) shows similar trends for double-sided heating. One significant difference is that, while a stable orientation region is predicted with single-sided heating at $U = 0.5$ m/s, this region is nonexistent for double-sided heating at 0.5 m/s, but is encountered at a lower velocity of 0.25 m/s. These differences can be attributed to double-sided heating producing more vapor and resulting in higher flow acceleration, which causes inertia to dwarf gravity effects at lower velocities than for single-sided heating.

4.5. Effects of orientation on CHF

Fig. 8(a) shows, for a range of velocities, a polar plot of CHF predictions with orientation relative to Earth gravity for single-sided heating. Notice how the influence of orientation is more pronounced for lower velocities and gradually abates with increasing velocity. The lowest CHF values in this figure correspond to $\theta = 225°$, which is consistent with experimental results [33,34] that showed this orientation to yield the worst CHF performance. Overall, CHF values are both highest and less sensitive to orientation for upflow and upward-facing heated wall orientations ($\theta = 0$–$90°$), and both significantly smaller and very sensitive to orientation for downflow and downward-facing heated wall orientations ($\theta = 180$–$270°$); the influence of orientation, especially for the latter range, is shown diminishing with increasing velocity.

Fig. 8(b) shows CHF polar plots for double-sided heating in Earth gravity. CHF predictions are shown for both upward-facing and downward-facing heated walls for all orientations. Recall that, during the experiments, power to the heated walls is cut off once either wall reaches CHF. But the *Interfacial Lift-off Model* is used here to predict CHF for both heated walls, which is useful to understanding the differences in underlying physical mechanisms between the two wall orientations. With reference to the flow orientation nomenclature, Fig. 8(b) distinguishes CHF for upward-facing and downward-facing heated walls using solid and dashed line, respectively. Notice how, as shown earlier in Fig. 6(b), a heated wall that is upward-facing for $\theta = 45°$, $0°$, and $315°$ becomes downward-facing for $\theta = 135°$, $180°$ and $225°$, and visa versa, which explains the symmetry in Fig. 8(b). Each double-sided heating orientation includes two heated walls that are subjected to opposite gravity components, and CHF is lower for a downward-facing wall than one upward-facing. This behavior is explained by buoyancy tending to remove vapor away from the upward-facing wall and

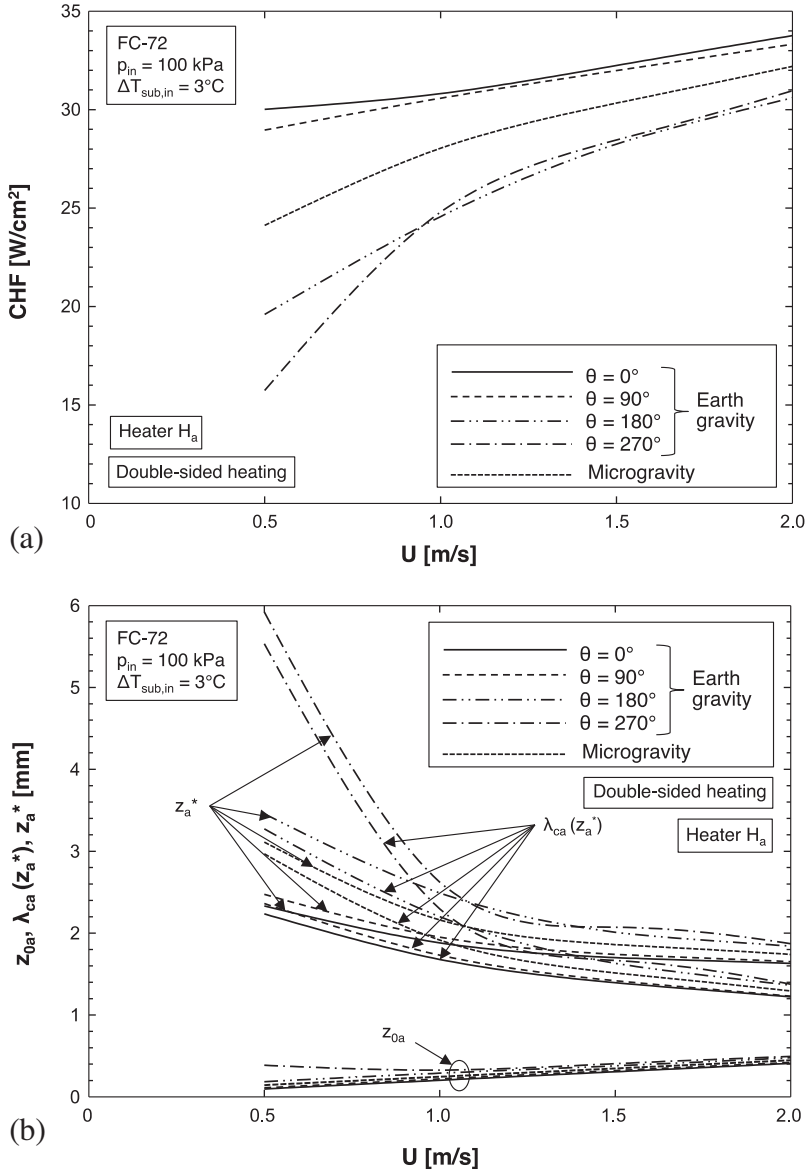

Fig. 10. Variations of (a) CHF and (b) z_{0a}, λ_{ca} (z_a^*) and z_a^* versus inlet velocity for heater wall H_a in double-sided heating in Earth gravity and microgravity.

towards the downward-facing wall, and decreasing liquid access to the latter. Increasing velocity is shown increasing CHF for both upward-facing and downward-facing walls, and the difference between the two wall orientations also decreases with increasing velocity, ultimately leading to convergence of CHF values for both wall orientations at high velocities.

Fig. 9(a) and (b) show alternative representations of CHF predictions over the entire range of orientations in Earth gravity, as well as in micro-gravity for single-sided heating and double-sided heating, respectively. For microgravity, orientation effects are inconsequential and CHF values are shown falling between the maxima and minima for Earth gravity. This is an important finding since it implies that performing terrestrial experiments for the entire range of orientations will provide a CHF range that encompasses that for microgravity at the same velocity. Moreover, CHF value for microgravity at a given velocity is close to the mean for all terrestrial orientations, and the microgravity and mean terrestrial values converge with increasing velocity. For double-sided heating, Fig. 9(b) shows the predicted CHF for microgravity and for heated walls H_a and H_b as well as minimum of the two for Earth gravity; the minimum is the value anticipated in actual experiments since power input to both walls is cut off once CHF is detected in either wall. While this plot shows results already presented in polar coordinates in Fig. 8(b), it provides additional details concerning the specific heated walls H_a and H_b independently at different orientations in Earth gravity as well as in microgravity. Notice how heated walls H_a and H_b in Earth gravity switch between upward-facing and downward-facing at $\theta = 90°$ and 270°.

It is also useful to examine the influences of velocity and orientation on important parameters of *Interfacial Lift-off Model*. These parameters are examined with respect to heated wall H_a during double-sided heating to demarcate the influences of gravity on both flow orientation and heated wall orientation. Figs. 10(a) shows the variation of CHF with inlet velocity. It shows CHF increases with increasing U, with orientations in the range of $\theta = 0–90°$ clearly out-performing $\theta = 180–270°$. This confirms what was stated earlier, that upflow with upward-facing heated wall orientations out-performs downflow with doward-facing orienta-

tions, but CHF values tend to converge with increasing U. CHF values for microgravity fall midway between the maxima and minima for Earth gravity.

Fig. 10(b) shows variations of computed values for other parameters of the *Interfacial Lift-off Model* with U. They include streamwise distance, z_{0a}, where $U_g = U_f$, extent of continuous upstream wetting region, z_a^*, and critical wavelength, $\lambda_{ca}(z_a^*)$. z_{0a} is both quite small and increases very slowly with increasing U, proving that the vapor velocity surpasses the liquid velocity very close to the upstream edge of the heated wall. Both z_a^* and $\lambda_{ca}(z_a^*)$ are shown decreasing with increasing U. These two parameters are highest at $\theta = 270°$, followed by 180°, 90° and 0°. Like CHF, the magnitudes of both parameters for different orientations tend to converge with increasing U. Here too, the parameters for microgravity fall midway between the maxima and minima for different orientations in Earth gravity. Overall, Fig. 10(a) and (b) point to the need to increase velocity above ~1.5 m/s to negate the influence of orientation in Earth gravity.

These findings clearly demonstrate the effectiveness of the *Interfacial Lift-off Model* in describing interfacial behavior at CHF– as well as the trigger event for CHF for both Earth gravity and microgravity. Further validation of the model may benefit from future experiments involving detailed tracking of the vapor-liquid interface as well as local, instantaneous velocity measurements as discussed in refs. [41,42].

5. Conclusions

This study is a consolidated investigation of the diverse and complex trends associated with flow boiling CHF in a rectangular channel in microgravity and for different orientations in Earth gravity. Several previous databases for FC-72 corresponding to slightly subcooled inlet conditions are used to assess the accuracy of the *Interfacial Lift-off Model* in capturing the CHF trends for both single-sided and double-sided wall heating. Key findings from the study are as follows.

(1) The *Interfacial Lift-off Model* shows good accuracy in predicting experimental CHF data for both Earth gravity and microgravity with both single-sided and double-sided wall heating.
(2) For Earth gravity, CHF mechanism is highly sensitive to flow orientation at very low velocities, but is consistent with the wavy vapor layer depiction of the *Interfacial Lift-off Model* at higher velocities. The model predicts a stable vapor-liquid interface for flow orientations between $\theta = 180$ and 270° for $U < 1$ m/s for single-sided wall heating, and $U < 0.5$ m/s for double-sided heating. A wavy liquid–vapor interface is predicted for all other orientations and velocities, the critical wavelength for which decreases with increasing velocity and become independent of orientation above ~1.5 m/s.
(3) For single-sided heating in Earth gravity, predicted CHF values for upflow with an upward-facing heated wall ($\theta = 0$–90°) are greater than those for downflow with a downward-facing wall ($\theta = 180$–270°). For double-sided heating, lower CHF is predicted for downward-facing than upward-facing walls.
(4) CHF values for microgravity fall about midway between the maxima and minima for Earth gravity. This is an important finding since it implies that, for a given inlet velocity, performing terrestrial experiments over the entire range of orientations will provide a range that encompasses CHF for microgravity.
(5) Overall, the *Interfacial Lift-off Model* shows that the values of CHF and key interfacial parameters for all orientations in Earth gravity and for microgravity converge together above ~1.5 m/s, where inertia begins to effectively negate gravity effects.

Acknowledgement

The authors are grateful for the support of this project by the National Aeronautics and Space Administration (NASA) under Grant No. NNX13AB01G.

References

[1] I. Mudawar, Two-phase micro-channel heat sinks: theory, applications and limitations, J. Electron. Packag. Trans. ASME 133 (2011). 041002-2.
[2] D.C. Wadsworth, I. Mudawar, Enhancement of single-phase heat transfer and critical heat flux from an ultra-high-flux-source to a rectangular impinging jet of dielectric liquid, J. Heat Transfer Trans. ASME 114 (1992) 764–768.
[3] D.D. Hall, I. Mudawar, Ultra-high critical heat flux (CHF) for subcooled water flow boiling – II. High-CHF database and design parameters, Int. J. Heat Mass Transfer 42 (1999) 1429–1456.
[4] M.K. Sung, I. Mudawar, Experimental and numerical investigation of single-phase heat transfer using a hybrid jet-impingement/micro-channel cooling scheme, Int. J. Heat Mass Transfer 49 (2006) 682–694.
[5] T.N. Tran, M.W. Wambsganss, D.M. France, Small circular- and rectangular-channel boiling with two refrigerants, Int. J. Multiphase Flow 22 (1996) 485–498.
[6] H.J. Lee, S.Y. Lee, Heat transfer correlation for boiling flows in small rectangular horizontal channels with low aspect ratios, Int. J. Multiphase Flow 27 (2001) 2043–2062.
[7] Y. Katto, H. Ohno, An improved version of the generalized correlation of critical heat flux for the forced convective boiling in uniformly heated vertical tubes, Int. J. Heat Mass Transfer 27 (1984) 1641–1648.
[8] D.C. Groeneveld, L.K.H. Leung, P.L. Kirillov, V.P. Bobkov, I.P. Smogalev, V.N. Vinogradov, X.C. Huang, E. Royer, The 1995 look-up table for critical heat flux in tubes, Nucl. Eng. Des. 163 (1996) 1–23.
[9] D.D. Hall, I. Mudawar, Critical heat flux (CHF) for water flow in tubes – I. Compilation and assessment of world CHF data, Int. J. Heat Mass Transfer 43 (2000) 2573–2604.
[10] D.D. Hall, I. Mudawar, Critical heat flux (CHF) for water flow in tubes – II. Subcooled CHF correlations, Int. J. Heat Mass Transfer 43 (2000) 2605–2640.
[11] C. Konishi, I. Mudawar, Review of flow boiling and critical heat flux in microgravity, Int. J. Heat Mass Transfer 80 (2015) 469–493.
[12] S.S. Kutateladze, A.I. Leont'ev, Some applications of the asymptotic theory of the turbulent boundary layer, in: Proc. 3rd Int. Heat Transfer Conf., vol. 3, Chicago, Illinois, 1966, pp. 1–6.
[13] J. Weisman, B.S. Pei, Prediction of critical heat flux in flow boiling at low qualities, Int. J. Heat Mass Transfer 26 (1983) 1463–1477.
[14] C.H. Lee, I. Mudawar, A mechanistic critical heat flux model for subcooled flow boiling based on local bulk flow conditions, Int. J. Multiphase Flow 14 (1988) 711–728.
[15] J.E. Galloway, I. Mudawar, CHF mechanism in flow boiling from a short heated wall – part 1. Examination of near-wall conditions with the aid of photomicrography and high-speed video imaging, Int. J. Heat Mass Transfer 36 (1993) 2511–2526.
[16] J.E. Galloway, I. Mudawar, CHF mechanism in flow boiling from a short heated wall – part 2. Theoretical CHF model, Int. J. Heat Mass Transfer 36 (1993) 2527–2540.
[17] F.P. Chiaramonte, J.A. Joshi, Workshop on critical issues in microgravity fluids, transport, and reaction processes in advanced human support technology – final report, NASA TM-2004-212940, 2004.
[18] The National Academies, Recapturing a Future for Space Exploration: Life and Physical Sciences Research for a New Era, National Academies Press, Washington, DC, 2011.
[19] A.E. Dukler, J.A. Fabre, J.B. McQuillen, R. Vernon, Gas–liquid flow at microgravity conditions: flow patterns and their transitions, Int. J. Multiphase Flow 14 (1988) 389–400.
[20] C. Colin, A. Kamp, J. Fabre, Influence of gravity on void distribution in two-phase gas–liquid flow in pipe, Adv. Space Res. 13 (1993) 141–145.
[21] T.R. Reinarts, Adiabatic two phase flow regime data and modeling for zero and reduced (horizontal flow) acceleration fields (Ph.D. thesis), Texas A&M University, TX, 1993.
[22] W.S. Bousman, Studies of two-phase gas–liquid flow in microgravity (Ph.D. thesis), University of Houston, TX, 1994.
[23] W.S. Bousman, J.B. McQuillen, L.C. Witte, Gas–liquid flow patterns in microgravity: effects of tube diameter, liquid viscosity and surface tension, Int. J. Multiphase Flow 22 (1996) 1035–1053.
[24] B. Choi, T. Fujii, H. Asano, K. Sugimoto, A study of gas–liquid two-phase flow in a horizontal tube under microgravity, Ann. N.Y. Acad. Sci. 974 (2002) 316–327.
[25] M. Misawa, An experimental and analytical investigation of flow boiling heat transfer under microgravity conditions (Ph.D. thesis), University of Florida, 1993.
[26] M. Saito, N. Yamaoka, K. Miyazaki, M. Kinoshita, Y. Abe, Boiling two-phase flow under microgravity, Nucl. Eng. Des. 146 (1994) 451–461.
[27] H. Ohta, Experiments on microgravity boiling heat transfer by using transparent heaters, Nucl. Eng. Des. 175 (1997) 167–180.
[28] D. Brutin, V.S. Ajaev, L. Tadrist, Pressure drop and void fraction during flow boiling in rectangular minichannels in weightlessness, Appl. Therm. Eng. 51 (2013) 1317–1327.

[29] Y. Ma, J.N. Chung, An experimental study of critical heat flux (CHF) in microgravity forced-convection boiling, Int. J. Multiphase Flow 27 (2001) 1753–1767.
[30] A.H. Howard, I. Mudawar, Orientation effects on pool boiling CHF and modeling of CHF for near-vertical surfaces, Int. J. Heat Mass Transfer 42 (1999) 1665–1688.
[31] D.E. Maddox, I. Mudawar, Single- and two-phase convective heat transfer from smooth and enhanced microelectronic heat sources in a rectangular channel, J. Heat Transfer Trans. ASME 111 (1989) 1045–1052.
[32] T.C. Willingham, I. Mudawar, Forced-convection boiling and critical heat flux from a linear array of discrete heat sources, Int. J. Heat Mass Transfer 35 (1992) 2879–2890.
[33] H. Zhang, I. Mudawar, M.M. Hasan, Experimental and theoretical study of orientation on flow boiling CHF, Int. J. Heat Mass Transfer 45 (2002) 4463–4477.
[34] C. Konishi, I. Mudawar, M.M. Hasan, Investigation of the influence of orientation on critical heat flux for flow boiling with two-phase inlet, Int. J. Heat Mass Transfer 61 (2013) 176–190.
[35] C.R. Kharangate, L. O'Neill, I. Mudawar, M.M. Hasan, H.K. Nahra, R. Balasubramaniam, N.R. Hall, A.M. Macner, J.R. Mackey, Flow boiling and critical heat flux in horizontal channel with one-sided and double-sided heating, Int. J. Heat Mass Transfer 90 (2015) 323–338.
[36] C.R. Kharangate, L. O'Neill, I. Mudawar, M.M. Hasan, H.K. Nahra, R. Balasubramaniam, N.R. Hall, A.M. Macner, J.R. Mackey, Effects of subcooling and two-phase inlet on flow boiling heat transfer and critical heat flux in a horizontal channel with one-sided and double-sided heating, Int. J. Heat Mass Transfer 91 (2015) 1187–1205.
[37] H. Zhang, I. Mudawar, M.M. Hasan, Investigation of interfacial behavior during the flow boiling CHF transient, Int. J. Heat Mass Transfer 47 (2004) 1275–1288.
[38] H. Zhang, I. Mudawar, M.M. Hasan, Flow boiling CHF in microgravity, Int. J. Heat Mass Transfer 48 (2005) 3107–3188.
[39] C. Konishi, H. Lee, I. Mudawar, M.M. Hasan, H.K. Nahra, N.R. Hall, J.D. Wagner, R.L. May, J.R. Mackey, Flow boiling in microgravity: Part 1 – Interfacial behavior and experimental heat transfer results, Int. J. Heat Mass Transfer 81 (2015) 705–720.
[40] C. Konishi, H. Lee, I. Mudawar, M.M. Hasan, H.K. Nahra, N.R. Hall, J.D. Wagner, R.L. May, J.R. Mackey, Flow boiling in microgravity: Part 2 – Critical heat flux interfacial behavior, experimental data, and model, Int. J. Heat Mass Transfer 81 (2015) 721–736.
[41] T.H. Lyu, I. Mudawar, Statistical investigation of the relationship between interfacial waviness and sensible heat transfer to a falling liquid film, Int. J. Heat Mass Transfer 34 (1991) 1451–1464.
[42] W. Qu, I. Mudawar, S.-Y. Lee, S.T. Wereley, Experimental and computational investigation of flow development and pressure drop in a rectangular micro-channel, J. Electron. Packag. Trans. ASME 128 (2006) 1–9.